Schweizerischer Erdbebendienst
Service Sismologique Suisse
Servizio Sismico Svizzero
Servizi da Terratrembels Svizzer

ETH
Eidgenössische Technische Hochschule Zürich
Swiss Federal Institute of Technology Zurich

Schaffhausen - Spital (SCHS)

SITE CHARACTERIZATION REPORT

Clotaire MICHEL, Valerio POGGI, Jan BURJANEK

Carlo CAUZZI, Daniel ROTEN, Donat FÄH

Sonneggstrasse 5 CH-8092 Zürich Switzerland; E-mail: clotaire.michel@sed.ethz.ch

Last modified : November 5, 2013

Abstract

Ambient vibration array measurements were performed on the site of the cantonal hospital in Schaffhausen, located on the hill above the city. The site is hosting station SCHS of the Swiss Strong Motion Network, which replaces the station SCHE from the old network, located in the industrial zone. In order to characterize the velocity profile under the station SCHS, two array configurations were performed with an aperture up to $100\,\mathrm{m}$. The measurements were successful in deriving a velocity model for this site that can be considered as a rock site. At the station SCHS, we found a layer of consolidated moraine of 12 to $17\,\mathrm{m}$ with a shear wave velocity of about $700\,\mathrm{m/s}$ overlaying limestone rock with V_s increasing from 1500 up to $3000\,\mathrm{m/s}$. The contrast between moraine and limestone is related to an ellipticity peak at $12\,\mathrm{Hz}$, whereas a deeper resonance at $0.6\,\mathrm{Hz}$ could be highlighted but not included in the model. It could be the interface between the Jurassic sedimentary rock and the crystalline basement. $V_{s,30}$ is found to be close to $960\,\mathrm{m/s}$, corresponding to a rock site (soil class A) for engineering purposes. The 1D amplification prediction shows a peak amplification around $10\,\mathrm{Hz}$.

Contents

1 Introduction **4**

2 Experiment description **5**

2.1 Ambient Vibrations 5

2.2 Equipment 5

2.3 Geometry of the arrays 5

2.4 Positioning of the stations 6

3 Data quality **7**

3.1 Usable data 7

3.2 Data processing 7

4 H/V processing **8**

4.1 Processing method and parameters 8

4.2 Results 8

5 Array processing **11**

5.1 Processing methods and parameters 11

5.2 Obtained dispersion curves 11

6 Inversion and interpretation **14**

6.1 Inversion 14

6.2 Travel time average velocities and ground type 18

6.3 SH transfer function and quarter-wavelength velocity 18

7 Conclusions **21**

References **23**

1 Introduction

The station SCHS (Schaffhausen Spital) is part of the Swiss Strong Motion Network (SSMNet) in the Northern part of Switzerland. SCHS was installed in the framework of the SSMNet Renewal project in 2011, replacing the SCHE (Schaffhausen Ebnat) dial-up station. This project includes also the site characterization. The passive array measurement has been selected as a standard tool to investigate these sites. Such a measurement campaign has been carried out on 22nd September 2011 in the Kantonsspital Schaffhausen (Fig. 1), with a centre at the station SCHS, in order to characterize the sediments under this station. According to the geological map, this station is located on a moraine terrace of the Würm and Riss ice-ages, between $10 - 30\,\mathrm{m}$ above the limestone basement, dipping to the South-East ("Plattenkalke", Ulmensis layer, White Jura, mid. Kimmeridge). This moraine terrace is located above the Rhine valley and the city of Schaffhausen. This report presents the measurement setup, the results of the H/V analysis, including the fundamental frequencies and of the array processing of the surface waves (dispersion curves). Then, an inversion of these results for a velocity profile is performed and inverted profiles are interpreted in terms of layering and amplification.

Canton	City	Location	Station code	Site type	Slope
Schaffhausen	Schaffhausen	Kantonsspital	SCHS	Rock Plateau	Flat

Table 1: Main characteristics of the study-site.

Figure 1: Picture of the site.

2 Experiment description

2.1 Ambient Vibrations

The ground surface is permanently subjected to ambient vibrations due to:

- natural sources (ocean and large-scale atmospheric phenomena) below $1\,\mathrm{Hz}$,
- local meteorological conditions (wind and rain) at frequencies around $1\,\mathrm{Hz}$,
- human activities (industrial machines, traffic…) at frequencies above $1\,\mathrm{Hz}$ [Bonnefoy-Claudet et al., 2006].

The objective of the measurements is to record these ambient vibrations and to use their propagation properties to infer the underground structure. First, the polarization of the recorded waves (H/V ratio) is used to derive the resonance frequencies of the soil column. Second, the arrival time delays at many different stations are used to derive the velocity of surface waves at different frequencies (dispersion). The information (H/V, dispersion curves) is then used to derive the properties of the soil column using an inversion process.

2.2 Equipment

For these measurements 12 Quanterra Q330 dataloggers named NR01 to NR12 and 14 Lennartz 3C 5 s seismometers were available (see Tab. 2). Each datalogger can record on 2 ports A (channels EH1, EH2, EH3 for Z, N, E directions) and B (channels EH4, EH5, EH6 for Z, N, E directions). Time synchronization was ensured by GPS. Each sensor is placed on a metal tripod in a $20\,\mathrm{cm}$ deep hole, when possible, for better coupling with the ground.

Digitizer	**Model**	**Number**	**Resolution**
	Quanterra Q330	12	$24\,\mathrm{bits}$
Sensor type	**Model**	**Number**	**Cut-off frequency**
Velocimeter	Lennartz 3C	14	$0.2\,\mathrm{Hz}$

Table 2: Equipment used.

2.3 Geometry of the arrays

Two array configurations were used, for a total of 4 rings of 7, 15, 30 and $50\,\mathrm{m}$ radius around a central station. The first configuration includes the 3 inner rings with 14 sensors; the second configuration includes the 2 outer rings (plus the first ring) with 14 sensors. The minimum inter-station distance and the aperture are therefore 7 and $60\,\mathrm{m}$ and 7 and $100\,\mathrm{m}$, respectively. The experimental setup is displayed in Fig. 2. The final usable datasets are detailed in section 3.2.

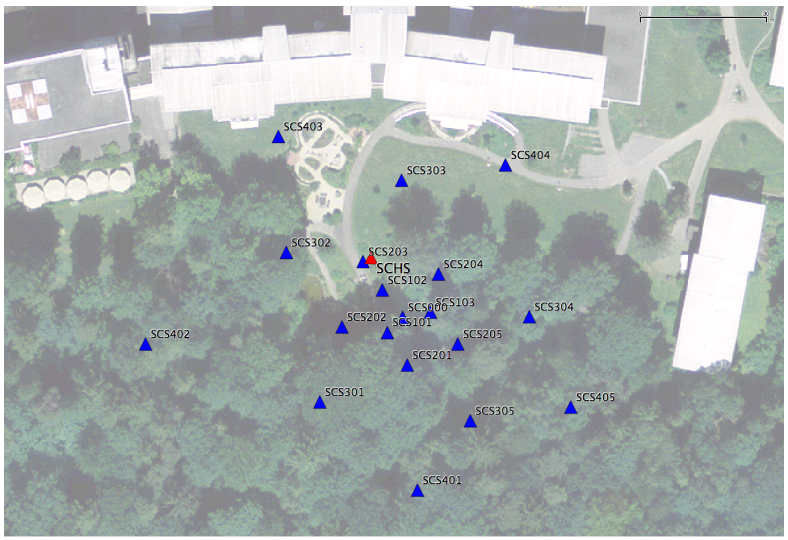

Figure 2: Geometry of the arrays.

2.4 Positioning of the stations

The sensor coordinates were measured using a differential GPS device (Leica Viva), including only a rover station and using the Real Time Kinematic technique provided by Swisstopo. It allows an absolute positioning with an accuracy of about $3\,\mathrm{cm}$ on the Swissgrid. However, the system worked only for points in the open field. For points in the forest, 3 to 5 minutes GPS recordings were performed and post-processed using a virtual reference provided by Swisstopo (RINEX data) and the LGO software. The accuracy of location is variable but better than $20\,\mathrm{cm}$ in this case. Longer GPS recording might have improved the accuracy.

3 Data quality

3.1 Usable data

The largest time windows were extracted, for which all the sensors of the array were in position and the GPS synchronization was ensured. GPS measurement were performed during the beginning of the first recording and the end of the second but these recording periods were not removed from the datasets. Points SCS102, SCS203 and SCS303 are probably set close to the pipes providing water to the fountain of the small artificial lake located in the array. Machines are disturbing the measurement (sharp peaks in the spectra) especially at frequencies: $7.46, 7.74, 13.44, 13.85$ and $24.49\,\mathrm{Hz}$. Looking at the spectra in each direction, point SCS000 shows higher amplitude at low frequency in the horizontal directions compared to the other points, whereas SCS303 shows higher amplitudes at higher frequencies (higher than $4\,\mathrm{Hz}$). The characteristics of the datasets are detailed in Tab. 3.

3.2 Data processing

The data were first converted to SAC format including in the header the sensor coordinates (CH1903 system), the recording component and a name related to the position. The name is made of 3 letters characterizing the location (SCS here), 1 digit for the ring and 2 more digits for the number in the ring. Recordings were not corrected from the instrumental response.

Dataset	**Starting Date**	**Time**	**Length**	F_s	**Min. inter-distance**	**Aperture**	**# of points**
1	2011/09/22	10:16	$135\,\mathrm{min}$	$200\,\mathrm{Hz}$	$7\,\mathrm{m}$	$60\,\mathrm{m}$	14
2	2011/09/22	13:13	$122\,\mathrm{min}$	$200\,\mathrm{Hz}$	$7\,\mathrm{m}$	$100\,\mathrm{m}$	14

Table 3: Usable datasets.

4 H/V processing

4.1 Processing method and parameters

In order to process the H/V spectral ratios, several codes and methods were used. The classical H/V method was applied using the Geopsy `http://www.geopsy.org` software. In this method, the ratio of the smoothed Fourier Transform of selected time windows is averaged. Tukey windows (cosine taper of 5% width) of $50\,\mathrm{s}$ long overlapping by 50% were selected. Konno and Ohmachi [1998] smoothing procedure with b=80 was used. The classical method computed using the method of Fäh et al. [2001] was also performed.

Moreover, the time-frequency analysis method [Fäh et al., 2009] was used to estimate the ellipticity function more accurately using the Matlab code of V. Poggi. In this method, the time-frequency analysis using the Wavelet transform is computed for each component. For each frequency, the maxima over time (10 per minute with at least $0.1\,\mathrm{s}$ between each) in the TFA are determined. The Horizontal to Vertical ratio of amplitudes for each maximum is then computed and statistical properties for each frequency are derived. Cosine wavelet with parameter 9 is used. The mean of the distribution for each frequency is stored. For the sake of comparison, the time-frequency analysis by Fäh et al. [2001], based on the spectrogram, was also used, as well as the wavelet-based TFA coded in Geopsy.

The ellipticity extraction using the Capon analysis [Poggi and Fäh, 2010] was also performed and displayed on Fig. 4 (See section on array analysis for details).

Method	Freq. band	Win. length	Anti-trig.	Overlap	Smoothing
Standard H/V Geopsy	$0.2 - 20\,\mathrm{Hz}$	$50\,\mathrm{s}$	No	50%	K&O 80
Standard H/V D. Fäh	$0.2 - 20\,\mathrm{Hz}$	$30\,\mathrm{s}$	No	75%	?
H/V TFA Geopsy	$0.2 - 20\,\mathrm{Hz}$	Morlet m=8 fi=1	No	-	?
H/V TFA D. Fäh	$0.2 - 20\,\mathrm{Hz}$	Specgram	No	-	?
H/V TFA V. Poggi	$0.2 - 20\,\mathrm{Hz}$	Cosine wpar=9	No	-	No

Table 4: Methods and parameters used for the H/V processing.

4.2 Results

H/V curves using time-frequency analysis are consistent for all the recordings (Fig. 3). Moreover, all the methods to compute H/V ratios are compared on Fig. 4, in which the classical methods were arbitrarily divided by $\sqrt{2}$ [Fäh et al., 2001]. The matching is reasonable. However, the first peak is not easy to determine around $0.6\,\mathrm{Hz}$, with a peak amplitude around 2. It corresponds to a deep interface in the rock. It is however not used in the following because its depth is likely to be very large compared to what is resolved here. At higher frequencies, sharp peaks are disturbing the H/V, though a second peak appears around $12\,\mathrm{Hz}$. It corresponds to a shallow layer that can be explored with the performed array, whereas the deep resonance cannot be analyzed with this too small configuration. Mapping this second peak along the array (Fig. 5) shows little variations: points close to the building appear to have a lower frequency but it is probably due to soil-structure interaction. The other points do not show significant

differences that could be related to the South-East dipping of the limestone bedrock described the geological map. The ellipticity extracted from the 3C FK processing shows a much clearer peak at a value of $13.5\,\mathrm{Hz}$ but a lower amplitude (around 2.2).

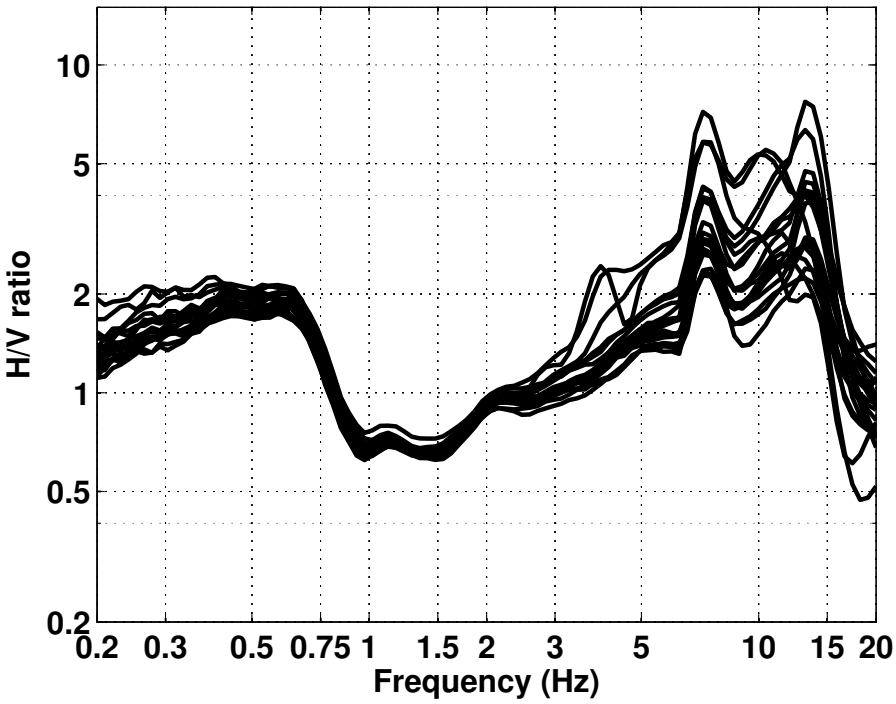

Figure 3: H/V spectral ratios (time-frequency analysis code V. Poggi).

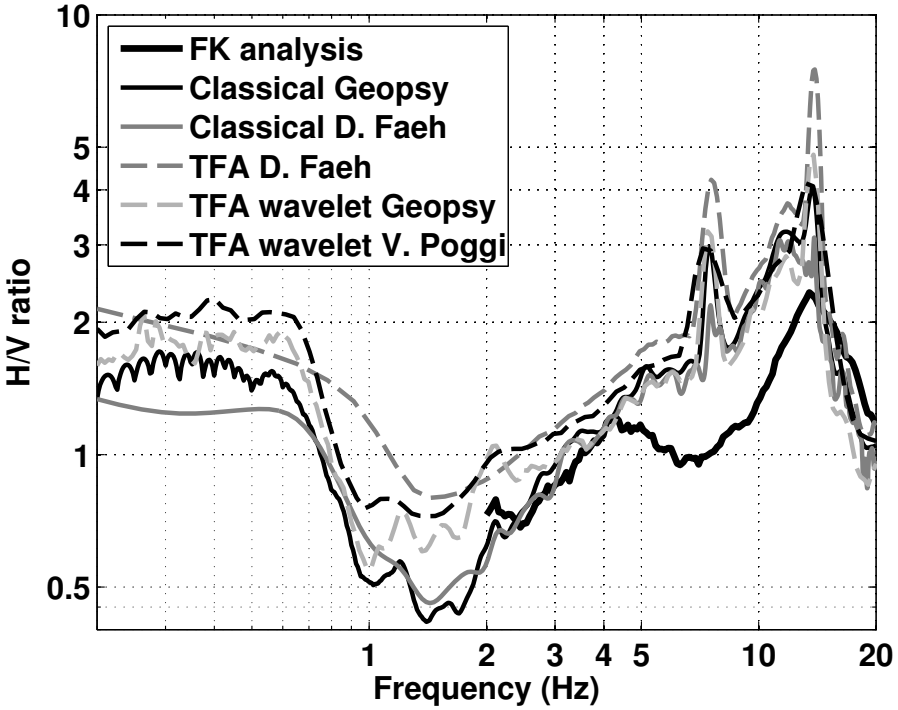

Figure 4: H/V spectral ratios for point SCS000 using the different codes. Classical methods were divided by $\sqrt{2}$.

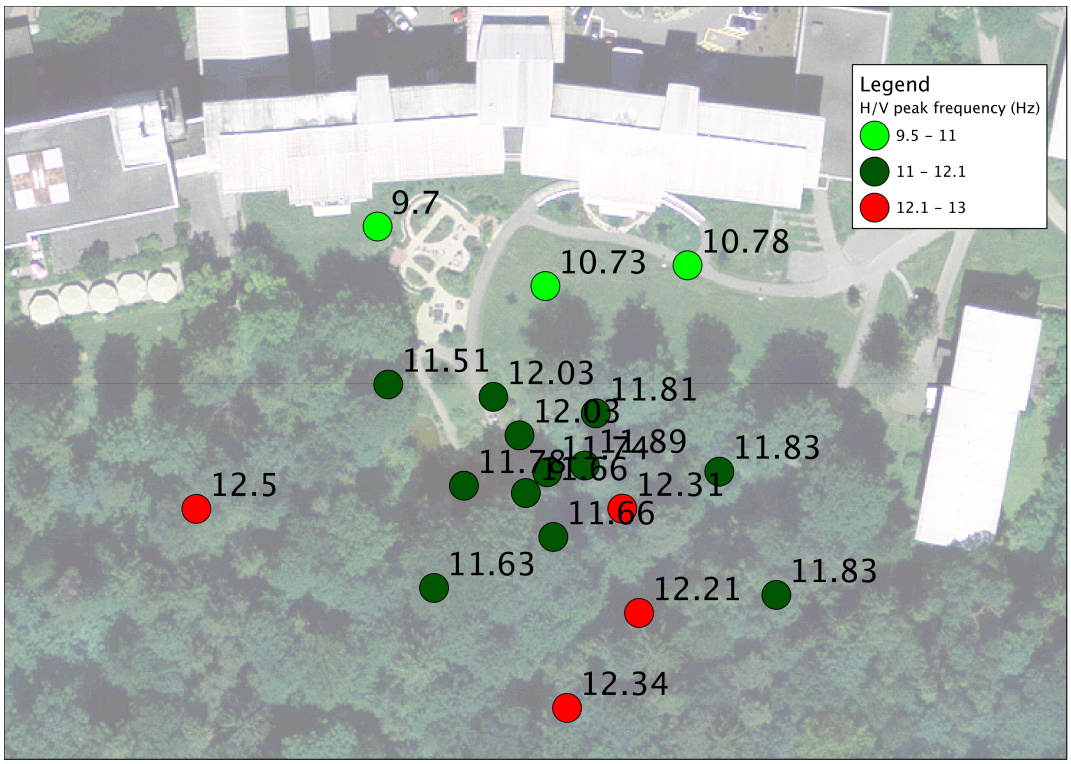

Figure 5: Map of the resonance frequency of the surface layer using time-frequency analysis code V. Poggi.

5 Array processing

5.1 Processing methods and parameters

The vertical components of the arrays were processed using the High-resolution FK analysis [Capon, 1969] using the Geopsy `http://www.geopsy.org` software. Better results were obtained using large time windows (300T, where T stands for period). Dispersion curves obtained from each dataset were concatenated.

Moreover, a 3C array analysis [Fäh et al., 2008] was also performed using the array_tool_3c software [Poggi and Fäh, 2010]. It allows to derive Rayleigh (including ellipticity) and Love modes. The results of computations of both datasets were merged to estimate the dispersion curves.

Method	Set	Freq. band	Win. length	Anti-trig.	Overlap	Grid step	Grid size	# max.
HRFK 1C	1	$5-40\,\mathrm{Hz}$	$300T$	No	50%	0.001	0.5	5
HRFK 1C	2	$5-40\,\mathrm{Hz}$	$300T$	No	50%	0.001	0.5	5
HRFK 3C	1	$2-30\,\mathrm{Hz}$	Wav. 10	No	50%	300	3000	5
			Tap. 0.2			m/s	m/s	
HRFK 3C	2	$2-30\,\mathrm{Hz}$	Wav. 10	No	50%	300	3000	5
			Tap. 0.2			m/s	m/s	

Table 5: Methods and parameters used for the array processing.

5.2 Obtained dispersion curves

A single mode has been picked in the 1C FK analysis between 9.5 and $23.5\,\mathrm{Hz}$ (Fig. 6) including its standard deviation. The dispersion curve can be followed below the lower array limit thanks to the Capon technique and the fact that there is still energy, even below the fundamental frequency. The velocities are ranging from $2000\,\mathrm{m/s}$ below $15\,\mathrm{Hz}$ down to $635\,\mathrm{m/s}$ at $23.5\,\mathrm{Hz}$.

Using the 3C analysis, both fundamental Rayleigh and Love modes can be picked (Fig. 7). The interpretation of the Rayleigh mode distribution is modified with respect to the 1C analysis considering both vertical and radial components. The fundamental Rayleigh mode is picked until $12\,\mathrm{Hz}$ on the vertical component and then on the radial component. A first higher Rayleigh mode is picked on the vertical component above $15\,\mathrm{Hz}$ (Fig. 8). On the transverse component, Love mode can be picked, though its energy remains low. It is close to the Rayleigh mode below $8\,\mathrm{Hz}$. Rayleigh fundamental mode is picked from 7 to $22.5\,\mathrm{Hz}$ and Love from 7 to $15\,\mathrm{Hz}$.

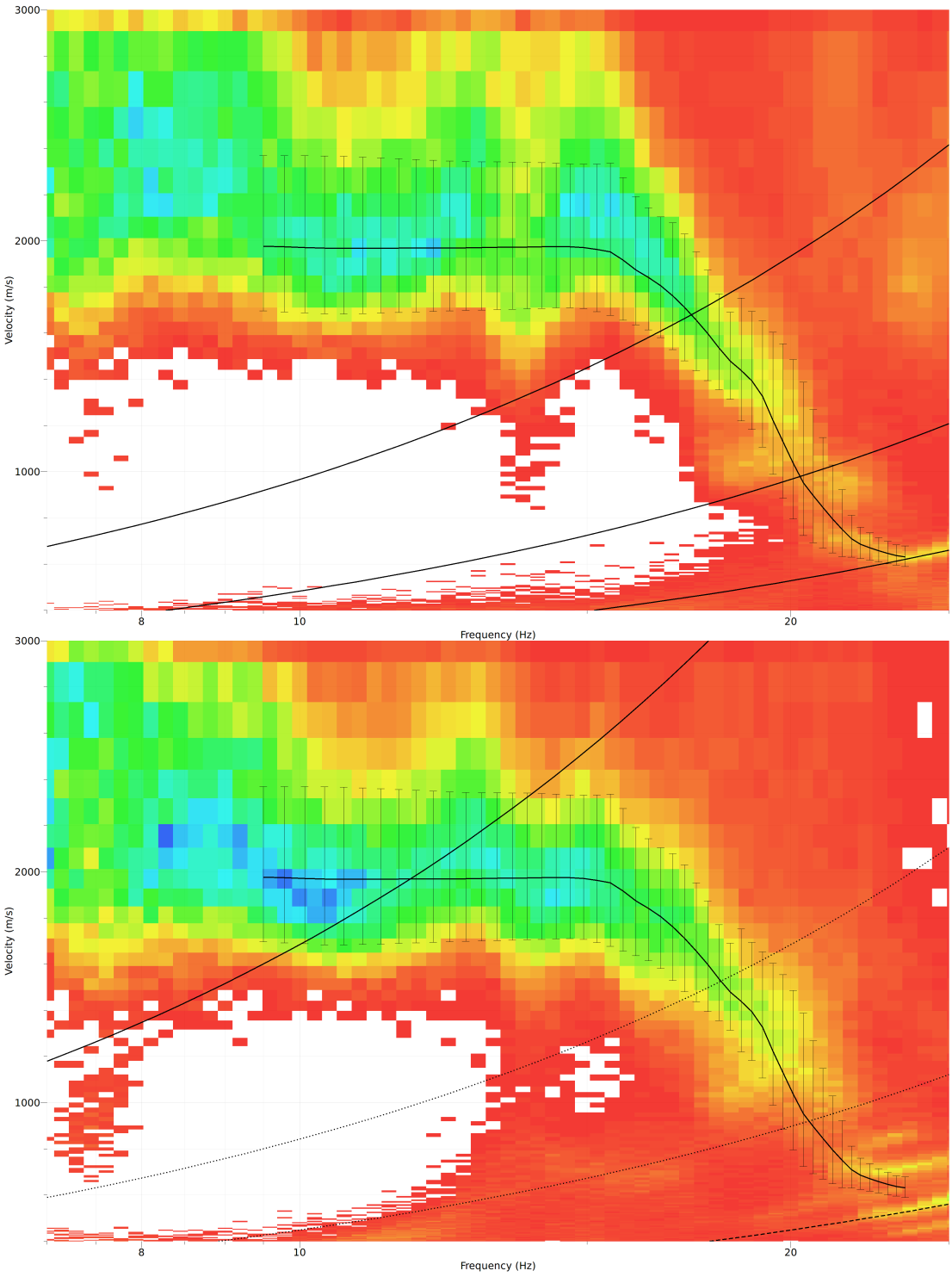

Figure 6: Dispersion curve obtained from the 1C array analysis (top: dataset 1, bottom: dataset 2).

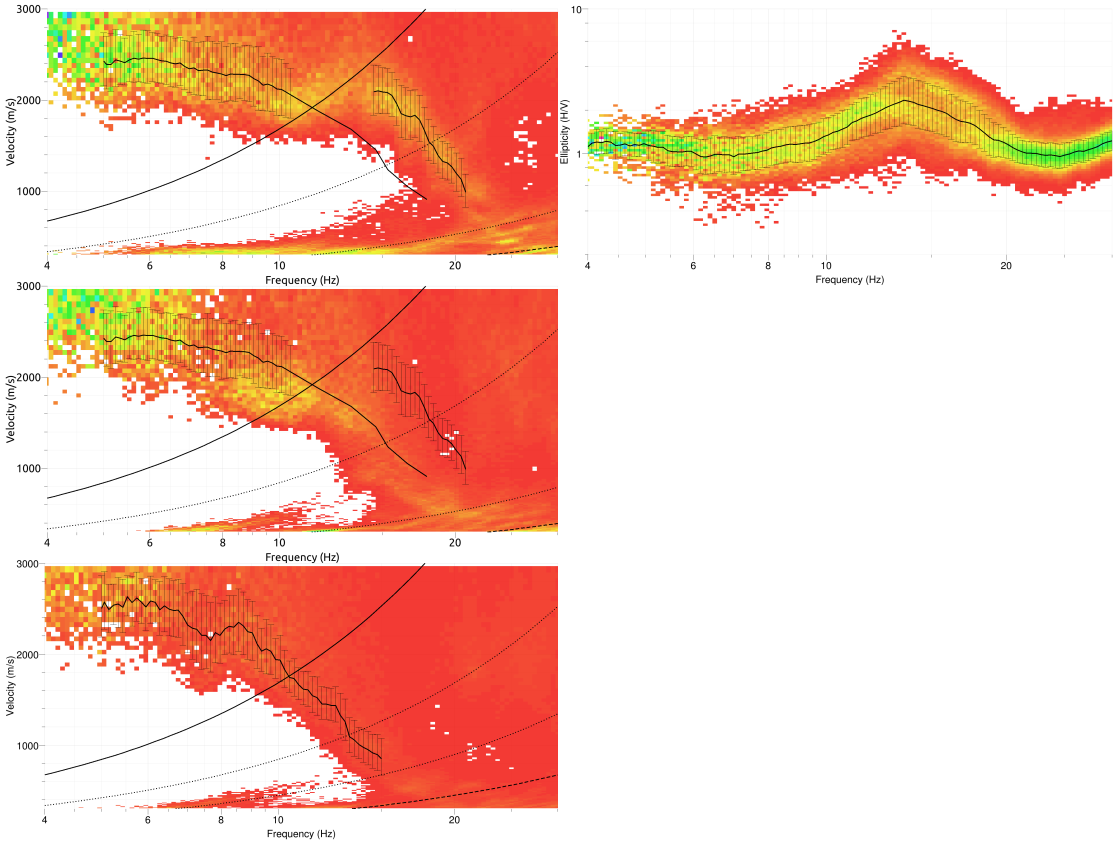

Figure 7: Results of the 3C array analysis on the vertical (top), radial (centre) and transverse (bottom) components for dispersion (left) and ellipticity (right).

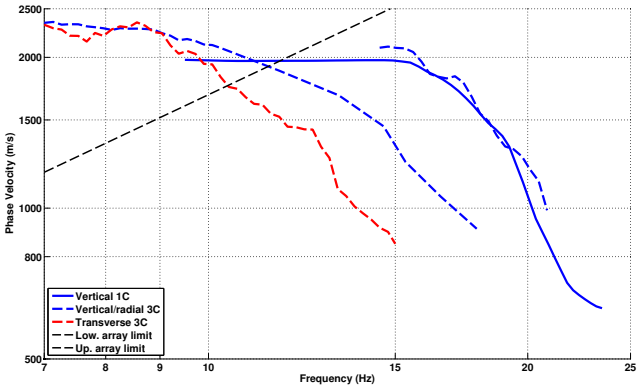

Figure 8: Picked dispersion curves from 1C and 3C analyses.

6 Inversion and interpretation

6.1 Inversion

For the inversion, the Love and the Rayleigh fundamental modes (3C analysis) and Rayleigh first higher mode dispersion curves without standard deviation to avoid different weighting between 7 and 15 Hz, 7 and 18 Hz and 15 and 20 Hz, respectively, were used. The inversion targets include as well the right flank of the ellipticity curve (TFA V. Poggi of point 203) and the peak of the ellipticity at point SCS203 (closest to station SCHS). A weight of 0.2 was assigned to the ellipticity information. All curves were resampled using 50 points between 7 and 25 Hz in log scale.

The inversion was performed using the Improved Neighborhood Algorithm (NA) Wathelet [2008] implemented in the Dinver software. In this algorithm, the tuning parameters are the following: Ns_0 is the number of starting models, randomly distributed in the parameter space, Nr is the the number of best cells considered around these Ns_0 models, Ns is the number of new cells generated in the neighborhood of the Nr cells (Ns/Nr per cell) and It_{max} is the number of iteration of this process. The process ends with $Ns_0 + Nr * \frac{Ns}{Nr} * It_{max}$ models. The used parameters are detailed in Tab. 6.

It_{max}	Ns_0	Ns	Nr
500	10000	100	100

Table 6: Tuning parameters of Neighborhood Algorithm.

During the inversion process, low velocity zones were not allowed. The Poisson ratio was supposed constant in each layer (in the range 0.2-0.4) and the density was supposed equal to $2000\,\mathrm{kg/m^3}$ for the sediments and $2500\,\mathrm{kg/m^3}$ for the rock layers. Inversions with free layer depths as well as fixed layer depths were performed. 3 layers are enough to explain most of the targets (dispersion and ellipticity), but more layers are used to smooth the obtained results and better explore the parameter space. 5 independent runs of 5 different parametrization schemes (2 and 4 layers over a half space and 10, 15 and 17 layers with fixed depth) were performed. For further elaborations, the best models of these 25 runs were selected (Fig. 11)..

In the first $2\,\mathrm{m}$, low velocities (down to $300\,\mathrm{m/s}$) are inverted (Fig. 9), but the velocity increases quickly to about $700\,\mathrm{m/s}$ down to 12 to $17\,\mathrm{m}$. This layer is likely to be the moraine terrace indicated by the geology. A this depth, a clear contrast with rock material is found (limestone from the geology). The retrieved velocity in the rock is 1500 to $3000\,\mathrm{m/s}$, likely increasing with depth as shown by the fixed-layer depth inverted profiles.

When comparing to the target curves (Fig. 9), the Love and Rayleigh dispersion curves are correctly represented in their major features, although the uncertainty remains large, especially on the points at higher frequency. The right flank of the ellipticity is reproduced.

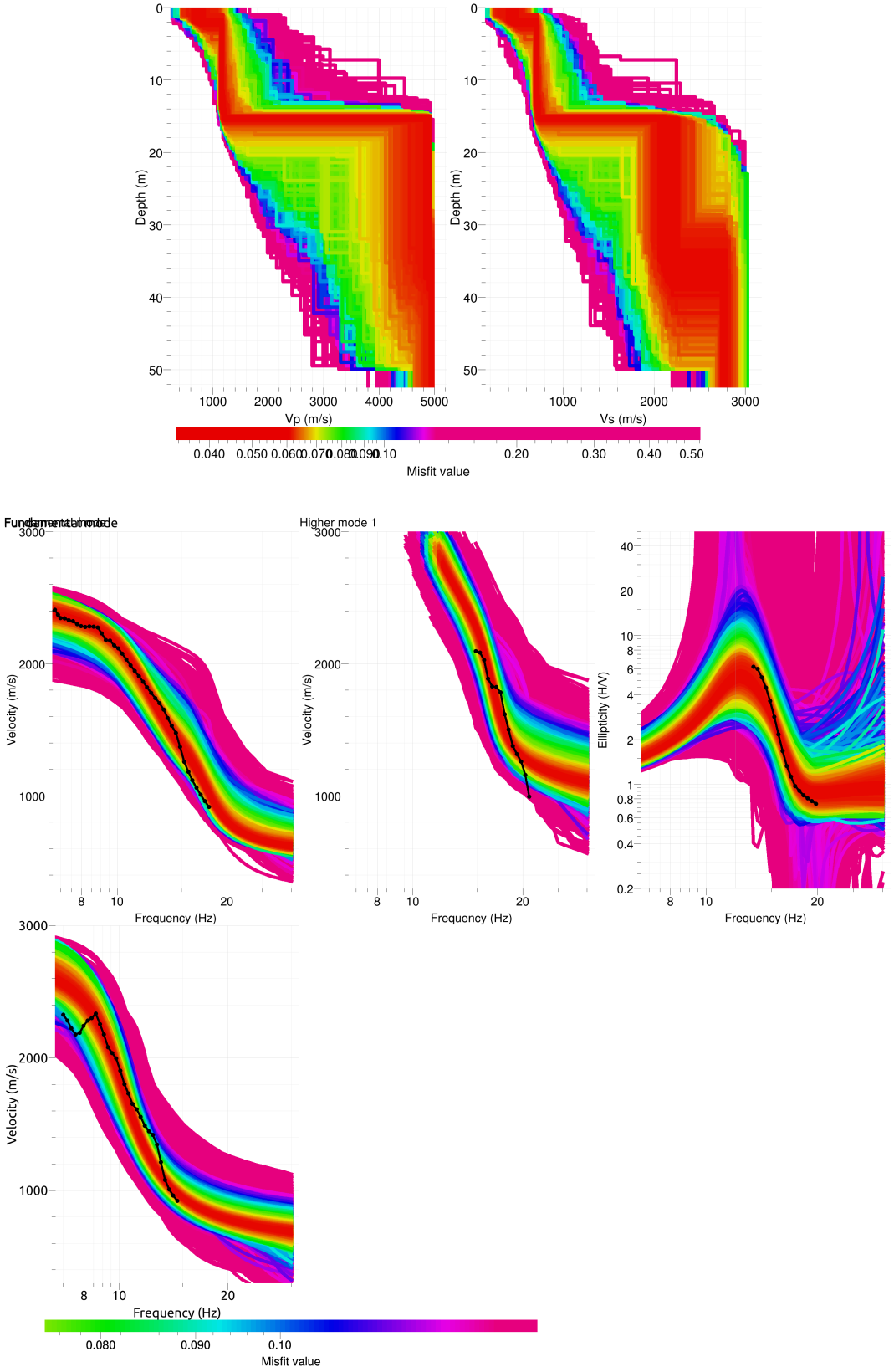

Figure 9: Inverted ground profiles in terms of V_p and V_s (top) and comparison between inverted models and measured Rayleigh and Love modes and corresponding ellipticity, free layer depth strategy.

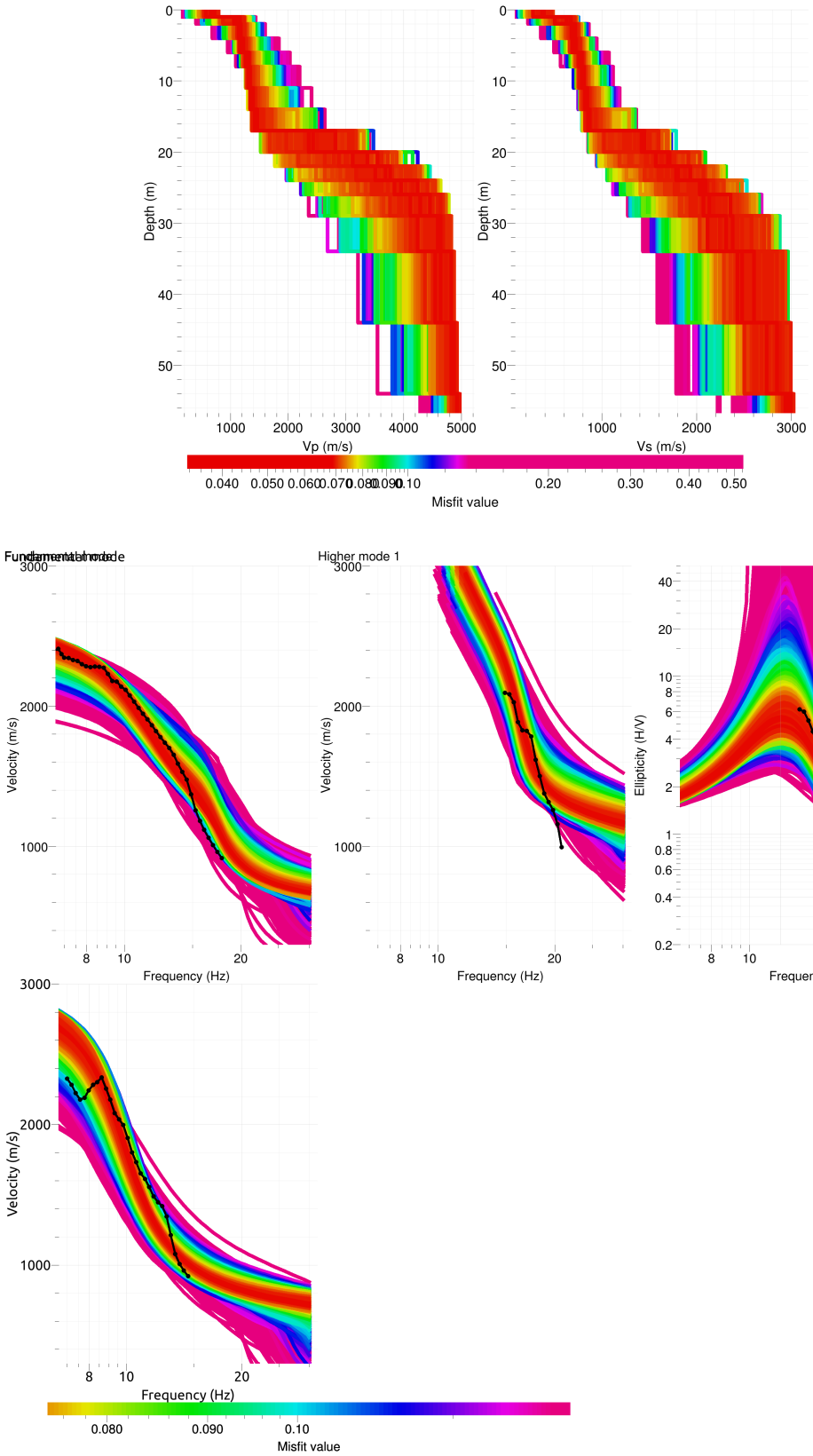

Figure 10: Inverted ground profiles in terms of V_p and V_s (top) and comparison between inverted models and measured Rayleigh and Love modes and corresponding ellipticity, fixed layer depth strategy.

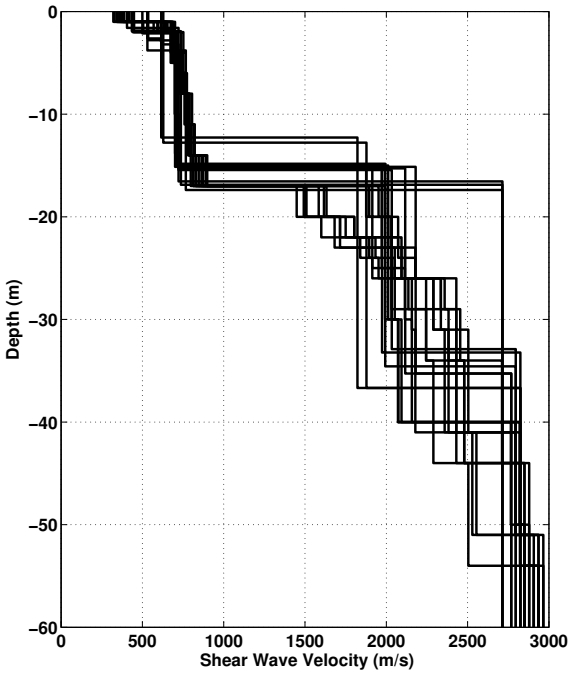

Figure 11: V_s ground profiles for the selected 25 best models.

6.2 Travel time average velocities and ground type

The distribution of the travel time average velocities at different depths was computed from the selected models. The uncertainty, computed as the standard deviation of the distribution of travel time average velocities for the considered models, is also provided, but its meaning is doubtful. $V_{s,30}$ is found to be $960\,\mathrm{m/s}$, meaning the site can be classified as class A in the Eurocode 8 [CEN, 2004] and SIA261 [SIA, 2003]. It cannot be classified in E since the upper layers are not more than $5\,\mathrm{m}$ deep with velocities lower than $500\,\mathrm{m/s}$ (SIA261), which is not fully determined.

	Mean (m/s)	**Uncertainty (m/s)**
$V_{s,5}$	584	19
$V_{s,10}$	646	15
$V_{s,20}$	778	36
$V_{s,30}$	960	89
$V_{s,40}$	1081	101
$V_{s,50}$	1190	138
$V_{s,100}$	-	-
$V_{s,150}$	-	-
$V_{s,200}$	-	-

Table 7: Travel time averages at different depths from the inverted models. Uncertainty is given as one standard deviation from the selected profiles.

6.3 SH transfer function and quarter-wavelength velocity

The quarter-wavelength proxy [Joyner et al., 1981] is providing the depth and velocity corresponding to each frequency for a given velocity profile (Fig. 12). It provides in particular the frequency limits of the experimental data (minimum frequency in the dispersion curves $7\,\mathrm{Hz}$). The results using this proxy mean that the dispersion curves constrain the results down to $40\,\mathrm{m}$. Moreover, the theoretical SH transfer function [Roesset, 1970] is computed from the inverted profiles. It is compared to the quarter-wavelet proxy for amplification, that however cannot take resonances into account [Joyner et al., 1981] (Fig. 13). The SH transfer function shows a peak amplification at $10.5\,\mathrm{Hz}$, whereas the quarter-wavelet proxy for amplification is smoother with amplification up to 2 at high frequencies. The station should therefore be considered as a rock station but with some limitations. This will be compared to observations. The first peak in the ellipticity curve at $0.6\,\mathrm{Hz}$ corresponds to a depth of around $1000\,\mathrm{m}$ (Fig. 12) and is therefore impossible to use in this inversion. This depth corresponds approximately to the interface between the Jurassic sedimentary rock and the crystalline basement [Sommaruga et al., 2012].

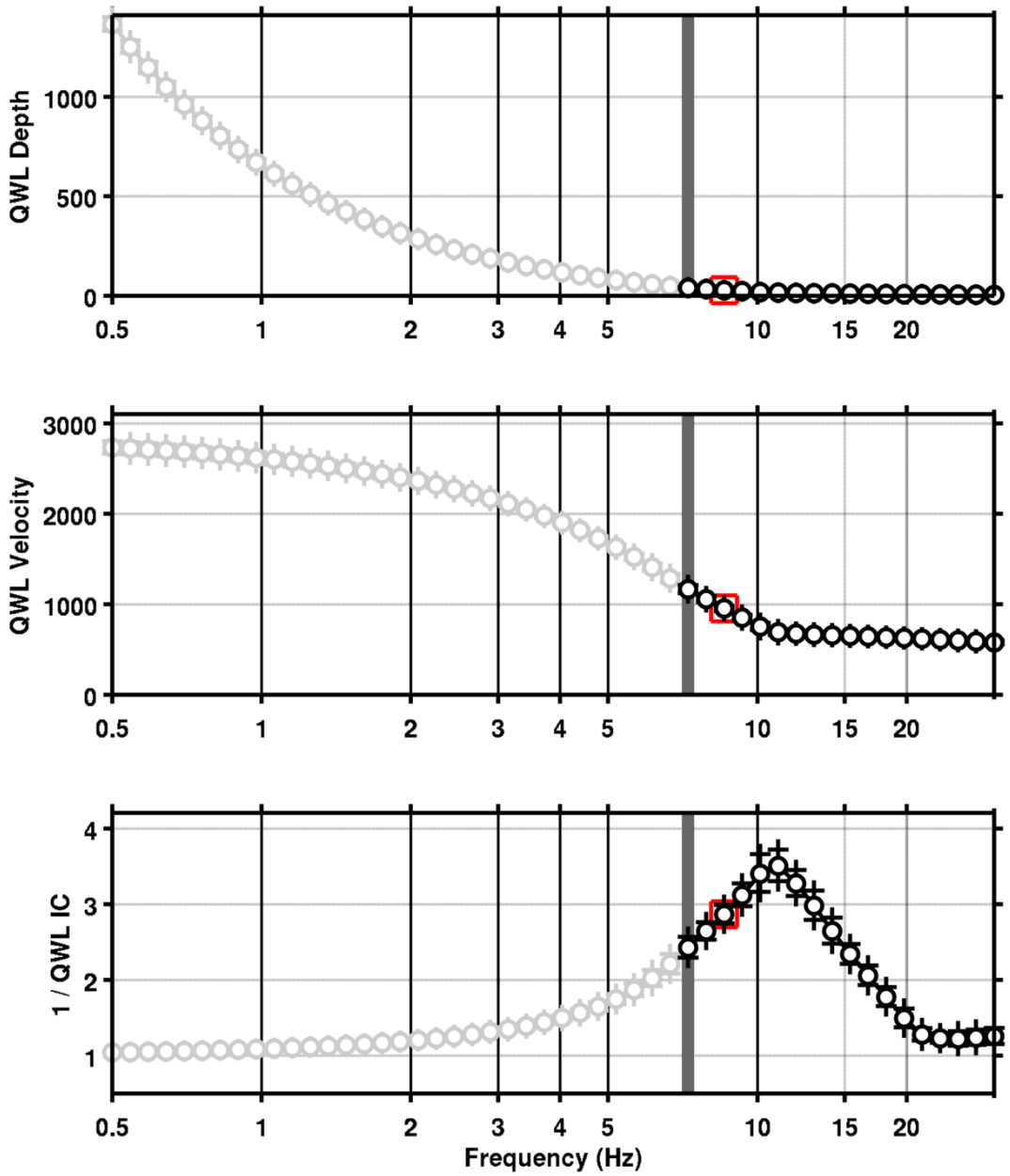

Figure 12: Quarter wavelength velocity representation of the velocity profile (top: depth, centre: velocity, bottom: inverse of the impedance contrast). Black curve is constrained by the dispersion curves, light grey is not constrained by the data. Red square is corresponding to $V_{s,30}$.

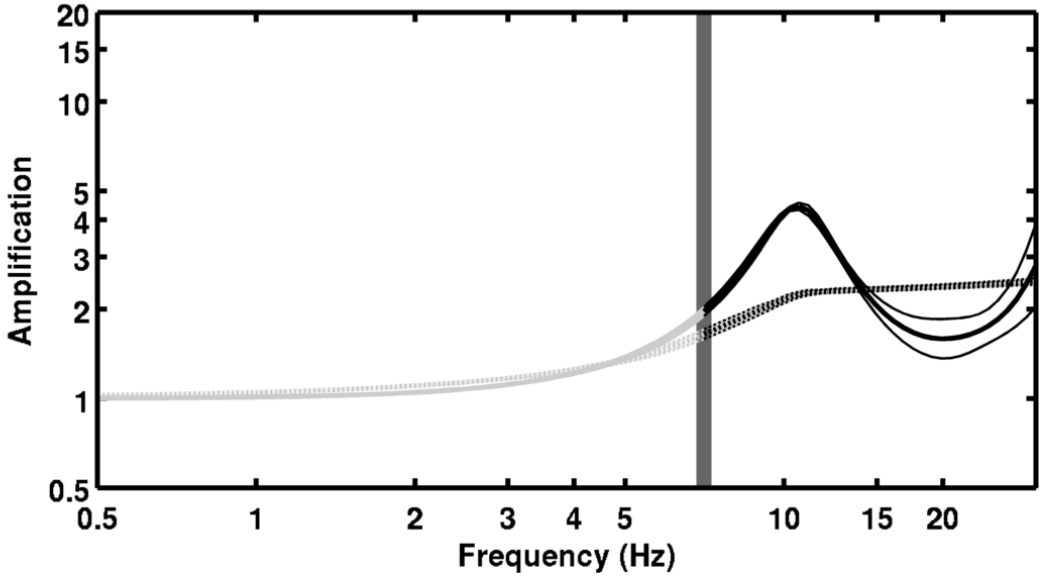

Figure 13: Theoretical SH transfer function (solid line) and quarter wavelength impedance contrast (dashed line) with their standard deviation. Significance of the greyshades is detailed in Fig. 12.

7 Conclusions

These array measurements were successful in deriving a velocity model for the hospital site in Schaffhausen. At the station SCHS, we found a layer of consolidated moraine of 12 to $17\,\mathrm{m}$ with a shear wave velocity of about $700\,\mathrm{m/s}$ overlaying limestone rock with V_s increasing from 1500 up to $3000\,\mathrm{m/s}$. This velocity contrast is responsible for an ellipticity peak at $12\,\mathrm{Hz}$, whereas a deeper resonance at $0.6\,\mathrm{Hz}$ could be highlighted but not included in the model. It could be the interface between the Jurassic sedimentary rock and the crystalline basement. $V_{s,30}$ is found to be close to $960\,\mathrm{m/s}$, corresponding to a rock site for engineering purposes (soil class A). A peak amplification is predicted around $10\,\mathrm{Hz}$ with a non-negligible amplitude. Recordings on the new station should show this high frequency amplification.

Acknowledgements

The authors thank Hr Luginbühl for the help giving access to the park of the hospital.

References

Sylvette Bonnefoy-Claudet, Fabrice Cotton, and Pierre-Yves Bard. The nature of noise wavefield and its applications for site effects studies. *Earth-Science Reviews*, 79(3-4): 205–227, December 2006. ISSN 00128252. doi: 10.1016/j.earscirev.2006.07.004. URL http://linkinghub.elsevier.com/retrieve/pii/S0012825206001012.

J. Capon. High-Resolution Frequency-Wavenumber Spectrum Analysis. *Proceedings of the IEEE*, 57(8):1408–1418, 1969.

CEN. *Eurocode 8: Design of structures for earthquake resistance - Part 1: General rules, seismic actions and rules for buildings*. European Committee for Standardization, en 1998-1: edition, 2004.

Donat Fäh, Fortunat Kind, and Domenico Giardini. A theoretical investigation of average H / V ratios. *Geophysical Journal International*, 145:535–549, 2001.

Donat Fäh, Gabriela Stamm, and Hans-Balder Havenith. Analysis of three-component ambient vibration array measurements. *Geophysical Journal International*, 172(1):199–213, January 2008. ISSN 0956540X. doi: 10.1111/j.1365-246X.2007.03625.x. URL http://doi.wiley.com/10.1111/j.1365-246X.2007.03625.x.

Donat Fäh, Marc Wathelet, Miriam Kristekova, Hans-Balder Havenith, Brigitte Endrun, Gabriela Stamm, Valerio Poggi, Jan Burjanek, and Cécile Cornou. Using Ellipticity Information for Site Characterisation Using Ellipticity Information for Site Characterisation. Technical report, NERIES JRA4 Task B2, 2009.

William B. Joyner, Richard E. Warrick, and Thomas E. Fumal. The effect of Quaternary alluvium on strong ground motion in the Coyote Lake, California, earthquake of 1979. *Bulletin of the Seismological Society of America*, 71(4):1333–1349, 1981.

Katsuaki Konno and Tatsuo Ohmachi. Ground-Motion Characteristics Estimated from Spectral Ratio between Horizontal and Vertical Components of Microtremor. *Bulletin of the Seismological Society of America*, 88(1):228–241, 1998.

Valerio Poggi and Donat Fäh. Estimating Rayleigh wave particle motion from three-component array analysis of ambient vibrations. *Geophysical Journal International*, 180(1):251–267, January 2010. ISSN 0956540X. doi: 10.1111/j.1365-246X.2009.04402.x. URL http://doi.wiley.com/10.1111/j.1365-246X.2009.04402.x.

J.M. Roesset. Fundamentals of soil amplification. In R. J. Hansen, editor, *Seismic Design for Nuclear Power Plants*, pages 183–244. M.I.T. Press, Cambridge, Mass., 1970. ISBN 978-0-262-08041-5. URL http://mitpress.mit.edu/catalog/item/default.asp?ttype=2\&tid=5998.

SIA. *SIA 261 Actions sur les structures porteuses*. Société suisse des ingénieurs et des architectes, Zürich, sia 261:20 edition, 2003.

A. Sommaruga, U. Eichenberger, and F. Marillier. Seismic Atlas of the Swiss Molasse Basin. *Matériaux pour la Géologie de la Suisse*, 44, 2012.

Marc Wathelet. An improved neighborhood algorithm: Parameter conditions and dynamic scaling. *Geophysical Research Letters*, 35(9):1–5, May 2008. ISSN 0094-8276. doi: 10.1029/2008GL033256. URL `http://www.agu.org/pubs/crossref/2008/2008GL033256.shtml`.